Coherent multichannel optical theorem: Quantum control of the total scattering cross section

Adrien Devolder, Timur V. Tscherbul, and Paul Brumer

Phys. Rev. A **105**, 052808 — Published 18 May 2022

DOI: 10.1103/PhysRevA.105.052808

Coherent multichannel optical theorem: Quantum control of the total scattering cross section

Adrien Devolder[1], Timur V. Tscherbul[2], and Paul Brumer[1]
[1] *Chemical Physics Theory Group, Department of Chemistry, and Center for Quantum Information and Quantum Control, University of Toronto, Toronto, Ontario, M5S 3H6, Canada*
[2] *Department of Physics, University of Nevada, Reno, NV, 89557, USA*
(Dated: April 28, 2022)

The optical theorem is a fundamental aspect of quantum scattering theory. Here, we generalize this theorem to the case where the incident scattering state is a superposition of internal states of the collision partners, introducing additional interference contributions and, e.g., providing a route to control the total integral cross section. As in its standard form, forward scattering plays an essential role in the multichannel optical theorem, but with interference terms being related to the inelastic forward scattering amplitudes *between* states in the initial superposition. Using the resultant control index, we show that extensive control is possible over ultracold collisions of oxygen molecules in their rovibrational ground states, and of ^{85}Rb-^{85}Rb collisions, promising systems for the first experimental demonstration of the quantum interference control of the total scattering cross section.

I. INTRODUCTION

The multichannel optical theorem is a remarkable result in scattering theory that relates the imaginary part of the elastic forward amplitude to the total scattering cross section [1, 2], a consequence of probability conservation during the scattering. No matter how complicated the scattering, all information about the total cross section is contained in the elastic forward scattering. Discovered first for light by Sellmeier [3] and Rayleigh [4], the optical theorem was subsequently extended to quantum mechanics by Feenberg [5] and Bohr et al.[6], and has been used in many areas, such as atomic, molecular and optical physics [7, 8], plasma physics [9], astrophysics [8], atmospheric physics [7, 8], nuclear physics[10–12] and high-energy physics [13].

The standard optical theorem assumes an initial pure state of fixed energy. Here we extend this theorem to a broader class of initial states, a superposition at a fixed energy that generates new and interesting interference contributions. We then demonstrate the utility of the coherent optical theorem in controlling the total scattering cross section. Examples of efficient control of ultracold atomic and molecular collisions are provided.

Over the past decades, progress in cooling techniques has enabled the creation of ultracold gases of atoms and molecules[14]. Nevertheless, loss of coherence is caused by collisions between the atoms/molecules and limits their use in quantum information science [15–18]. On the other hand, such collisions are essential for understanding ultracold chemistry [19, 20]. Fortunately, some ultracold collisions can be controlled due to the ability to fully define the internal states of the atoms/molecules, and due to the small value of the kinetic energy relative to the perturbations induced by external fields. As a consequence, the vast majority of ultracold control scenarios are based on external fields (magnetic, electric or optical) [21, 22], with molecules/atoms prepared in a well-defined internal state. In these strategies, the control knobs are the field parameters (strength, frequency, etc.).

However, this approach, as noted below, has deficiencies, motivating a different strategy. That is, the control of the internal degree of freedom at ultracold temperature enables the preparation of quantum superpositions of internal states that can be used to induce interferences between scattering amplitudes, in analogy with the double slit experiments [23, 24]. Then, instead of control via variation of field parameters, ultracold collisions are controlled by changing the nature of the initial superposition. The resultant effect on the system is the principle of coherent control [23].

In previous work, we demonstrated that the ultracold regime is ideal for coherent control and that control can be achieved for resonant processes such as collisional spin exchange [25], which can be completely suppressed (or activated), via destructive (constructive) interference. Control is achieved without persistent application of external perturbations. In particular, the collision partners (atoms or molecules) need not have electric and(/or) magnetic dipole moments to be coherently controlled. For example, collisions of nonmagnetic homonuclear molecules, like H_2 or Sr_2, could be manipulated. Moreover, the absence of external field could be important for high-precision measurements (for example with Sr_2 molecules [26, 27]) where suppressing external perturbations is significant.

At present, contrary to the unimolecular processes [28], the observation of coherent control of bimolecular processes is still an open experimental challenge due to a number of issues. First, the preparation of the initial superposition is experimentally challenging. Conditions on the coherent control of scattering events require either entanglement of the external and internal degrees of freedom [29–32], or superposition of degenerate magnetic sublevels (an m-superposition) [33]. However, recently, some progress has been made in preparing m-superpositions in H_2 molecules and its isotopologues

[34–36]. Secondly, our previous study of coherent control at ultralow temperatures [25] focused on state-to-state cross sections, and indicated a need for complicated coincidence measurements of the two scattered molecules [37, 38]. On the other hand, the total cross section, considered here, could be experimentally easier to measure and control. 0 Below we demonstrate the utility of the coherent multichannel theorem in controlling the total scattering cross section. The theorem allows to answer the following fundamental questions: How does the standard optical theorem generalize when the scattering is of an initial superposition of internal states? What are the new insights for coherent control of the total cross section arising from this generalization? And, with these new insights, can we identify atomic and/or molecular collisions promising for a first experimental demonstration of coherent control of the total scattering cross section? Answering these questions is important for the development of this completely new control strategy for ultracold collisions and for applications in other scattering scenarios.

The structure of the paper is as follows. We first derive the coherent multichannel optical theorem (Section II) and, in the rest of the paper, use the resultant theorem to address the control related issues raised above. In Section III, we compare the derived formulas with the standard form of the optical theorem. The coherent optical theorem allows us to define a coherent control index for the total integral cross section (ICS) in Section IV, which we then use to analyze promising systems for experiments in Section V. Exact scattering calculations are presented which show impressive control over the total cross section for the experimentally realizable ultracold ^{85}Rb-^{85}Rb and $^{17}O_2$-$^{17}O_2$ collisions. We conclude in section VI.

II. DERIVATION

Consider an initial superposition of N_{sup} degenerate internal states of the scattering partners denoted $|i\rangle = |\nu_A\rangle |\nu_B\rangle$. Here $\nu_{A,B}$ are the quantum numbers characterizing the internal states of the molecular or atomic collision partners A+B. The initial state is:

$$\Psi_{in}(\vec{r},\xi) = \mathrm{e}^{ikz} \sum_{i=1}^{N_{sup}} a_i |i\rangle , \tag{1}$$

where the z-axis is defined along the initial relative momentum $\vec{k}$. Here a_i are the superposition coefficients, $\vec{r} = (r,\theta,\phi)$ is the relative position between the two collision partners, and ξ is composed of all internal coordinates contained in $|i\rangle$.

After the collision, the system is in a superposition of scattered spherical waves in all open channels [1]:

$$\Psi_{out}(\vec{r},\xi) = \sum_j f_{sup\to j}(\theta,\phi)\frac{\mathrm{e}^{ik_j r}}{r} |j\rangle , \tag{2}$$

where k_j is the final relative momentum in the state $|j\rangle$ and

$$f_{sup\to j}(\theta,\phi) = \sum_{i=1}^{N_{sup}} a_i f_{i\to j}(\theta,\phi) \tag{3}$$

is the scattering amplitude from the initial superposition to the final state $|j\rangle$. Here, $f_{i\to j}$ is the scattering amplitude from state $|i\rangle$ to $|j\rangle$. The overall wavefunction therefore obeys the boundary condition:

$$\Psi(\vec{r},\xi) \xrightarrow[r\to\infty]{} \mathrm{e}^{ikz} \sum_{i=1}^{N_{sup}} a_i |i\rangle + \sum_j f_{sup\to j}(\theta,\phi)\frac{\mathrm{e}^{ik_j r}}{r} |j\rangle . \tag{4}$$

The optical theorem can be derived by imposing conservation of probability via the continuity equation:

$$\oint \vec{j}(\vec{r})\cdot\hat{e}_r r^2 d\Omega = 0, \tag{5}$$

where $\vec{j}(\vec{r}) = \int \mathrm{d}\xi \frac{\hbar}{2i\mu}\Psi^*(\vec{r},\xi)\vec{\nabla}\Psi(\vec{r},\xi) + \mathrm{c.c}$ is the current density, μ is the reduced mass, $\hat{e}_r$ is the unit radial vector, $d\Omega = \sin\theta \mathrm{d}\theta\mathrm{d}\phi$ is the solid angle, and c.c denotes complex conjugate. The continuity equation states that the scattering flux through any closed surface must vanish, which is also the case for a sphere with radius $r\to\infty$ where the boundary condition (4) is imposed. This flux, defined as $I \equiv \lim_{r\to\infty}\oint \vec{j}(\vec{r}).\hat{e}_r r^2 \mathrm{d}\Omega$, can be expanded into three terms: the incoming term I_{in}, the outgoing term I_{out} and the interference term I_{int}:

$$I_{in} + I_{out} + I_{int} = 0. \tag{6}$$

The terms I_{ini}, I_{out} and I_{int} are derived in the appendices A, B and C, respectively, and their final values are:

$$I_{in} = 0, \tag{7}$$

$$I_{out} = \frac{\hbar k}{\mu}\sigma_{sup}^{tot}, \tag{8}$$

$$I_{int} = \frac{-4\pi\hbar}{\mu}\sum_{i,i'=1}^{N_{sup}} \mathrm{Im}[a_i^* a_{i'} f_{i'\to i}(\theta=0)]. \tag{9}$$

Introducing (7),(8) and (9) in Eq. (6), one obtains the total integral cross section (ICS):

$$\sigma_{sup}^{tot} = \frac{4\pi}{k}\sum_{i,i'=1}^{N_{sup}} \mathrm{Im}[a_i^* a_{i'} f_{i'\to i}(\theta=0)]. \tag{10}$$

Consider then the dependence of the total cross section on the relative phases β_i between the states of the initial superposition, which can be explicitly illustrated

by writing the superposition coefficients in their polar form: $a_i = |a_i|e^{i\beta_i}$:

$$\sigma_{sup}^{tot} = \frac{4\pi}{k}\sum_{i=1}^{N_{sup}} |a_i|^2 \mathrm{Im}[f_{i\to i}(\theta=0)] + \frac{4\pi}{k}\sum_{i}\sum_{i'\neq i} |a_i||a_{i'}| \mathrm{Im}\left[e^{i(\beta_{i'}-\beta_i)} f_{i'\to i}(\theta=0)\right]. \quad (11)$$

Finally, the symmetric relation between the scattering amplitudes $f_{i'\to i} = f_{i\to i'}$ can be exploited to obtain the coherent multichannel optical theorem:

$$\sigma_{sup}^{tot} = \frac{4\pi}{k}\sum_{i=1}^{N_{sup}} |a_i|^2 \mathrm{Im}[f_{i\to i}(\theta=0)] + \frac{8\pi}{k}\sum_{i=1}^{N_{sup}}\sum_{i'>i} |a_i||a_{i'}| \mathrm{Im}[f_{i\to i'}(\theta=0)]\cos(\beta_{i'}-\beta_i). \quad (12)$$

The symmetric form is valid when the time-reversal symmetry applies. When it does not, Eq. (11) should be used.

Equations (11) and (12) are the central result of this work. They establish a relation between the magnitude of the total ICS and the preparation coefficients of the internal superposition, enabling coherent control of the total ICS. Note that they are of the standard coherent control form [23], indirect scattering terms plus interference between pairs of states.

III. AN EXTENSION OF THE STANDARD OPTICAL THEOREM

The coherent multichannel optical theorem (Eq. 12) establishes the total ICS as composed of a direct contribution (upper line) and an interference contribution (lower line). The direct contribution is related to the elastic forward scattering amplitudes of individual states in the superposition, weighted by their populations. This contribution would be the same for a classical mixture with $|a_i|$ given, for example by Boltzmann populations. The standard optical theorem without superposition follows from the direct contribution in the limit $N_{sup} = 1$, $a_1 = 1$:

$$\sigma_1^{tot} = \frac{4\pi}{k}\mathrm{Im}[f_{1\to 1}(\theta=0)]. \quad (13)$$

For the purpose of control, the significance of the interference contribution is that it allows control over the total ICS by varying the amplitude product $|a_i||a_{i'}|$ and the relative phases $(\beta_{i'} - \beta_i)$ between the states in the initial superposition. The interference contribution is related to the inelastic forward scattering amplitudes *between* the states in the initial superposition, and is the primary attribute of the coherent multichannel optical theorem, corresponding to interference between scattering events in different channels. *It indicates that inelastic scattering between the channels involved in the initial superposition is a prerequisite for coherent control of total ICS.* Note that whatever the system, the interference terms oscillate as $\cos(\beta_{i'} - \beta_i)$ and, that contrary to the elastic component $\mathrm{Im}[f_{i\to i}(\theta=0)]$, the inelastic component $\mathrm{Im}[f_{i\to i'}(\theta=0)]$ can be negative.

Consider now the key quantity that determine the magnitude of the interference contribution to the total ICS, (**??**), the imaginary part of the inelastic forward scattering amplitude:

$$\mathrm{Im}[f_{i\to i'}(\theta=0)] = \frac{1}{4k}\sum_j \sum_{\ell',m'} \tilde{T}_{i\to j,\ell',m'} \tilde{T}^*_{i'\to j,\ell',m'}, \quad (14)$$

where $\tilde{T}_{i\to j,\ell',m'} = \sum_\ell i^\ell \sqrt{2\ell+1} T_{i,\ell,0\to j,\ell',m'}$, ℓ and ℓ' are the initial and final partial wave, and $T_{i,\ell,0\to j,\ell',m'}$ are the T-matrix elements. Equation (14) provides an important perspective, that is: *interference is a result of scattering of states $|i\rangle$ and $|i'\rangle$ into the same states j, ℓ', m'.* Further, the sum $\sum_j \sum_{\ell',m'} \tilde{T}_{i\to j,\ell',m'} \tilde{T}^*_{i'\to j,\ell',m'}$ is seen to be real. Equation (14) is required by conservation of probability and the coherent multichannel optical theorem can also be proven via this relation.

IV. COHERENT CONTROL OF THE TOTAL CROSS SECTION

A. Two-state superpositions

The coherent multichannel optical theorem allows for considerable new insights into the quantum control of the total ICS. First, consider the case where the initial superposition of the scattering partners is composed of two states, $\Psi_{in}(\vec{r},\xi) = e^{ikz}\left(\cos\eta\,|1\rangle + \sin\eta e^{i\beta}\,|2\rangle\right)$. Here, control is achieved by changing the amplitude and phase of the superposition by varying η and β, respectively. The theorem [Eq. (12)] then takes the form

$$\sigma_{sup}^{tot} = \frac{4\pi}{k}\{\cos^2(\eta)\mathrm{Im}[f_{1\to 1}] + \sin^2(\eta)\mathrm{Im}[f_{2\to 2}]\} + \frac{8\pi}{k}\cos\eta\,\sin\eta\,\mathrm{Im}[f_{1\to 2}]\cos\beta. \quad (15)$$

Insight is afforded by minimization and maximization of this expression. The optimization with respect to β is straightforward; maximal for $\cos\beta = 1$ ($\beta_{max} = 0$) and minimal for $\cos\beta = -1$ ($\beta_{max} = \pi$) if $\mathrm{Im}[f_{1\to 2}(\theta = 0)]$ is positive. It is the opposite if $\mathrm{Im}[f_{1\to 2}(\theta=0)]$ is negative. The optimization with respect to η gives:

$$\eta_{min} = \frac{1}{2}\arctan\left(\frac{2\,|\mathrm{Im}[f_{1\to 2}]|}{\mathrm{Im}[f_{2\to 2}] - \mathrm{Im}[f_{1\to 1}]}\right), \quad (16)$$

$$\eta_{max} = -\frac{1}{2}\arctan\left(\frac{2\,|\mathrm{Im}[f_{1\to 2}]|}{\mathrm{Im}[f_{2\to 2}] - \mathrm{Im}[f_{1\to 1}]}\right), \quad (17)$$

Introducing η_{min},β_{min}, η_{max} and β_{max} in the Eq. (15), one obtains the minimal and maximal values of the total ICS:

$$\sigma^{tot}_{min} = \frac{2\pi}{k}\left(\mathrm{Im}[f_{1\to1}] + \mathrm{Im}[f_{2\to2}]\right) - \frac{2\pi}{k}\sqrt{\left(\mathrm{Im}[f_{2\to2}] - \mathrm{Im}[f_{1\to1}]\right)^2 + 4\mathrm{Im}^2[f_{1\to2}]}, \tag{18}$$

$$\sigma^{tot}_{max} = \frac{2\pi}{k}\left(\mathrm{Im}[f_{1\to1}] + \mathrm{Im}[f_{2\to2}]\right) + \frac{2\pi}{k}\sqrt{\left(\mathrm{Im}[f_{2\to2}] - \mathrm{Im}[f_{1\to1}]\right)^2 + 4\mathrm{Im}^2[f_{1\to2}]}. \tag{19}$$

The extent of the control is determined by the magnitude of $\mathrm{Im}[f_{1\to2}]$, a quantity bounded between zero and $\sqrt{\mathrm{Im}[f_{1\to1}]\mathrm{Im}[f_{2\to2}]}$. That leads us to define a control index:

$$R_c = \frac{|\mathrm{Im}[f_{1\to2}]|}{\sqrt{\mathrm{Im}[f_{1\to1}]\mathrm{Im}[f_{2\to2}]}}, \tag{20}$$

which ranges from zero to one. When $R_c = 1$, the Schwartz equality ($|\mathrm{Im}[f_{1\to2}]| = \sqrt{\mathrm{Im}[f_{1\to1}]\mathrm{Im}[f_{2\to2}]}$) holds. In this case, the minimum value of the total cross section σ^{tot}_{min} vanishes while the maximal value is the sum of the total cross sections in absence of superposition, $\sigma^{tot}_{max} = \frac{4\pi}{k}\left(\mathrm{Im}[f_{1\to1}] + \mathrm{Im}[f_{2\to2}]\right) = \sigma^{tot}_1 + \sigma^{tot}_2$. Hence, the value of R_c allows us to quantify the extent of coherent control of the total ICS and interpret when systems display the maximum possible degree of control (which is realized for R_c=1). An example of complete control is the case of ideal resonance, [32], where the resonance occurs for all final states. Another favorable situation is when the number of channels significantly populated in a collision is equal to (or less than) the number of states in the superposition[39]. The latter case is illustrated below in the section V.

B. N_{sup}-state superpositions (N_{sup}>2)

The optimization can be generalized to a superposition of N_{sup} states via a procedure similar to that introduced in Ref. [39]. We define the matrix $\Sigma_{ij} = \frac{4\pi}{k}\mathrm{Im}[f_{i\to j}(\theta = 0)]$ and rewrite the coherent multichannel optical theorem (Eq. 12) as:

$$\sigma^{tot}_{sup} = \boldsymbol{a}^\dagger \boldsymbol{\Sigma} \boldsymbol{a}, \tag{21}$$

where $\boldsymbol{a}$ is a vector with the components a_i.

The optimization problem of finding σ^{tot}_{min} and σ^{tot}_{max} transforms to the solution of an eigenvalue equation for $\boldsymbol{\Sigma}$:

$$\boldsymbol{\Sigma}\boldsymbol{a} = \sigma^{tot}_{opt}\boldsymbol{a}, \tag{22}$$

where the optimized coefficients are the corresponding eigenvectors. The matrix $\boldsymbol{\Sigma}$ is block diagonal with respect to the symmetry of the scattering. For example, a superposition of states with different projections M_{int} of the total internal angular momentum does not display interference since the imaginary part of the inelastic scattering amplitude between these states is zero. Therefore, they occupy different blocks of the matrix $\boldsymbol{\Sigma}$. The resulting eigenvectors only contain the states with the same value of M_{int} and correspond to entangled superpositions thereof.

The best system controllability is obtained if the lowest eigenvalue of $\boldsymbol{\Sigma}$ is equal to zero; i.e. if the determinant of $\boldsymbol{\Sigma}$ is null. On the other hand, in absence of control, the determinant is equal to the product of the diagonal elements. Then, we can define a generalized control index R_c:

$$R_c = \sqrt[N]{1 - \frac{det(\boldsymbol{\Sigma})}{\prod_i \Sigma_{ii}}}, \tag{23}$$

For example, in the two-states case, the determinant is equal to $\mathrm{Im}[f_{1\to1}]\mathrm{Im}[f_{2\to2}] - (\mathrm{Im}[f_{1\to2}])^2$, and we recover expression (20). For the three states case, for example, the matrix $\boldsymbol{\Sigma}$ is then defined as:

$$\boldsymbol{\Sigma} = \frac{4\pi}{k}\begin{pmatrix} \mathrm{Im}[f_{1\to1}] & \mathrm{Im}[f_{1\to2}] & \mathrm{Im}[f_{1\to3}] \\ \mathrm{Im}[f_{1\to2}] & \mathrm{Im}[f_{2\to2}] & \mathrm{Im}[f_{2\to3}] \\ \mathrm{Im}[f_{1\to3}] & \mathrm{Im}[f_{2\to3}] & \mathrm{Im}[f_{3\to3}] \end{pmatrix}. \tag{24}$$

The determinant of this matrix is given by:

$$\det(\boldsymbol{\Sigma}) = \frac{4\pi}{k}\Big(\mathrm{Im}[f_{1\to1}]\Big(\mathrm{Im}[f_{2\to2}]\mathrm{Im}[f_{3\to3}] - \mathrm{Im}[f_{2\to3}]^2\Big) - \mathrm{Im}[f_{1\to2}]\Big(\mathrm{Im}[f_{1\to2}]\mathrm{Im}[f_{3\to3}] - \mathrm{Im}[f_{2\to3}]\mathrm{Im}[f_{1\to3}]\Big) + \mathrm{Im}[f_{1\to3}]\Big(\mathrm{Im}[f_{1\to2}]\mathrm{Im}[f_{2\to3}] - \mathrm{Im}[f_{2\to2}]\mathrm{Im}[f_{1\to3}]\Big)\Big). \tag{25}$$

Using the definition (23), the control index takes the form:

$$R_c = \sqrt[3]{\frac{R^{num}_c}{\mathrm{Im}[f_{1\to1}]\mathrm{Im}[f_{2\to2}]\mathrm{Im}[f_{3\to3}]}}, \tag{26}$$

where:

$$R^{num}_c = 2\mathrm{Im}[f_{1\to2}]\mathrm{Im}[f_{2\to3}]\mathrm{Im}[f_{1\to3}] - \mathrm{Im}[f_{1\to1}](\mathrm{Im}[f_{2\to3}])^2 - \mathrm{Im}[f_{2\to2}](\mathrm{Im}[f_{1\to3}])^2 - \mathrm{Im}[f_{3\to3}](\mathrm{Im}[f_{1\to2}])^2. \tag{27}$$

As stated previously, the value of R_c can be used to interpret systems and coherent superpositions that give large control of the total ICS, as is done in the next section. Specifically, R_c close to one indicates the most efficient coherent control.

V. SYSTEMS WITH EXTENSIVE CONTROL OF THE TOTAL CROSS SECTION

The theory above provides a foundation for coherent control of the total ICS. In the next section, we consider

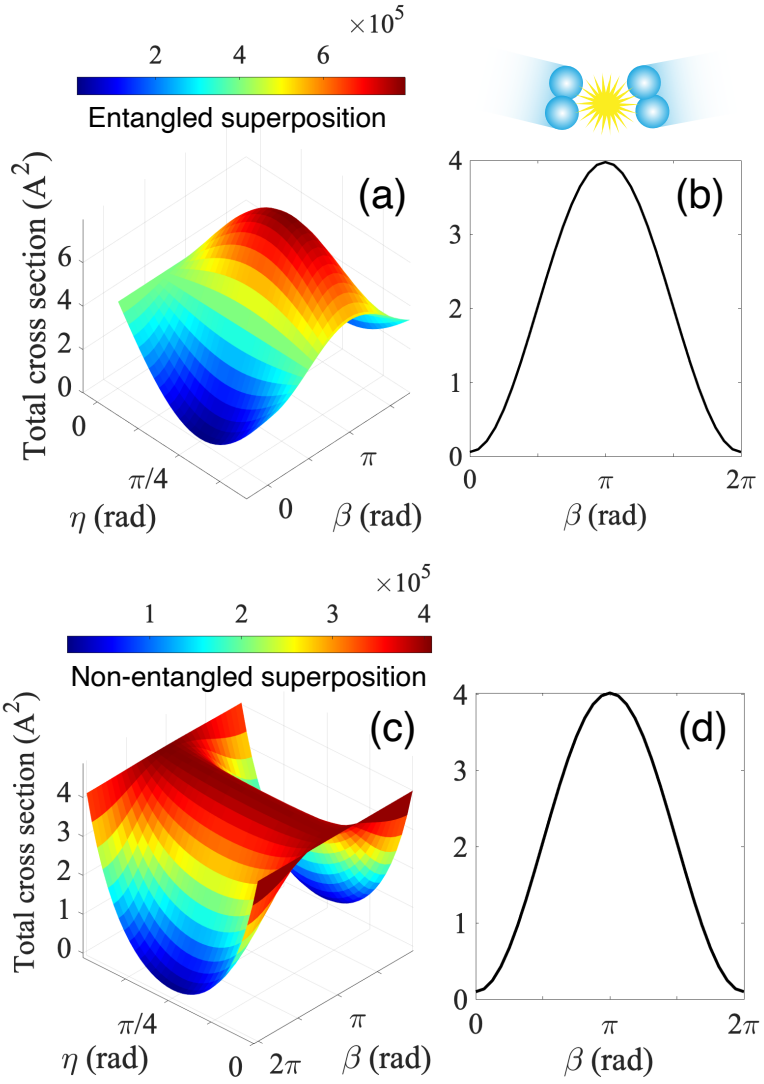

FIG. 1. Coherent control of the total integral cross section for the cold $^{17}O_2$+ $^{17}O_2$ collisions at 10 μK from the initial superposition Ψ_E (upper panels) and Ψ_{NE} (lower panels). (a) and (c): Control landscape; (b) and (d): Control by the relative phase β with $\eta = \pi/4$ fixed.

the coherent control of realistic atomic and molecular collisions at ultralow temperatures. In particular, we demonstrate the possibility of extensive coherent control of total ICS for O_2+O_2 and Rb+Rb collisions. Note that although the two examples correspond to collisions of indistinguishable particles, the derived optical theorem is general and valid for collisions between either indistinguishable or distinguishable particles.

A. O_2+O_2 scattering

The first system considered is ultracold scattering of two oxygen molecules in their rovibrational ground states at 10 μK. This system has been realized experimentally in a magnetic trap at 50 mK [40], with further evaporative or sympathetic cooling projected to achieve the μK regime. Hence, it is an advantageous system for study. The oxygen molecules have spin 1, and a spin-exchange processes can occur during the scattering. Our calculations neglect the hyperfine structure. In addition to computational practicability, there are some physical arguments to support it. First, the change of hyperfine state F requires a collisional energy of 3.7 mK and is forbidden at ultralow temperature. Second, the increase of the number of m-states (the lowest hyperfine state has $F = 6$) has pros and cons for the control. On the one hand, there are more final states to control. On the other hand, more states can be included in the initial superposition.

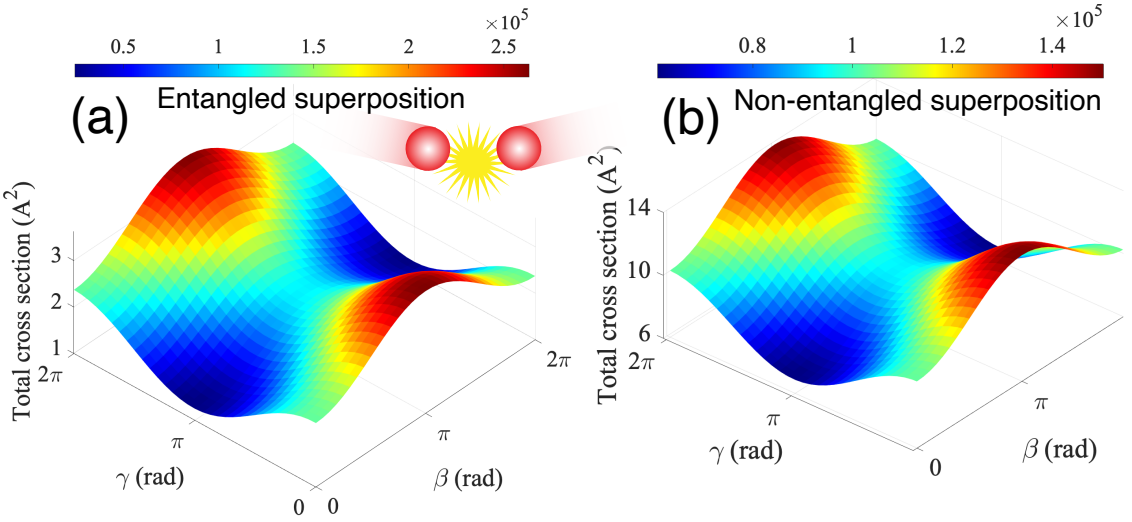

FIG. 2. Coherent control of the total cross section for the ultracold ^{85}Rb+^{85}Rb collisions in their lower hyperfine states $F = 2$ at 50 μK from the initial superpositions (a) Ψ_E and (b) Ψ_{NE}. The relative phases β, γ are varied, while the relative populations $\eta = 11\pi/32$, $\epsilon = 3\pi/8$ are fixed for achieving the best control.

The initial internal states considered here is an entangled superposition between the symmetrized states $|S_A = 1, M_{S_A} = -1, S_B = 1, M_{S_B} = 1\rangle$ and $|S_A = 1, M_{S_A} = 0, S_B = 1, M_{S_B} = 0\rangle$:

$$\Psi_E(\vec{r}, \xi) = \mathrm{e}^{ikz} \left(\cos\eta\, |1, -1, 1, 1\rangle + \sin\eta \mathrm{e}^{i\beta}\, |1, 0, 1, 0\rangle\right), \tag{28}$$

where $M_{S_{A/B}}$ is the projection of the electronic spin $S_{A/B}$ along the space-fixed z axis. The symmetrized initial states of identical bosons are defined as:

$$|S_1, m_1, S_2, m_2\rangle = \frac{1}{\sqrt{2(1+\delta_{1,2})}}\Big[\, |S_1, m_1\rangle_A\, |S_2, m_2\rangle_B + |S_2, m_2\rangle_A\, |S_1, m_1\rangle_B \,\Big], \tag{29}$$

where $m_2 \geq m_1$, and where the subscript on, for example, $|S_1, m_1\rangle_A$ denotes the states of particle A. At ultracold temperature, the main contribution in the total cross section only involves the s-wave. Including higher partial wave would, however, be necessary beyond 5 mK, reducing the control, as shown previously for the state-to-state cross sections [25].

The scattering results (see Appendix D for computational details) show that the control index is close to 1, i.e $R_c = 0.97$ (Im$[f_{1\to1}]$=158.96 a.u., Im$[f_{2\to2}]$=162.39 a.u. and Im$[f_{1\to2}]$=-156.00 a.u.). Figure 1 (a) shows the total ICS as a function of the relative population η and phase β of the initial superposition (28). The minimum value of the total ICS is seen to be 68 times smaller than the maximum value (11745 and 795427 Å^2, respectively), confirming the analysis in terms of the control index. This control can also be analyzed by decomposing the total cross section into the different state-to-state cross sections. The large extent of control can be explained by 3 points. First, in accord with the Wigner threshold law [41], only two final channels ($|1, -1, 1, 1\rangle$ and $|1, 0, 1, 0\rangle$) substantially contribute to the total cross section. Second, there is complete control of the state-to-state cross sections to these two channels, as illustrated in our earlier work [25]. Thirdly, the optimizing parameters are similar, allowing a simultaneous control for both final channel.

B. Rb+Rb scattering

A second system of interest is the ultracold scattering of ^{85}Rb atoms in their lower hyperfine states $F = 2$ at 50 μK. This system can be readily realized experimentally in either an optical dipole trap [42, 43] or an optical tweezer [44], allowing for precise control over internal and external atomic states. Here we consider s-wave scattering, consistent with our preliminary studies that showed that contributions from $l = 1$ partial waves contribute less that 4% at 50 μK. We first examine results for a scattering state prepared in an entangled superposition of three symmetrized states $|F_1 = 2, M_{F_1} = -2, F_2 = 2, M_{F_2} = 2\rangle$, $|F_1 = 2, M_{F_1} = -1, F_2 = 2, M_{F_2} = 1\rangle$ and $|F_1 = 2, M_{F_1} = 0, F_2 = 2, M_{F_2} = 0\rangle$:

$$\Psi_E(\vec{r}, \xi) = \mathrm{e}^{ikz}\Big(\cos\eta\, \sin\epsilon\, |2, -2, 2, 2\rangle + \sin\eta\, \sin\epsilon\, \mathrm{e}^{i\beta}\, |2, -1, 2, 1\rangle + \cos\epsilon\, \mathrm{e}^{i\gamma}\, |2, 0, 2, 0\rangle\Big). \tag{30}$$

Here, M_F denotes the projection of the total angular momentum $\vec{F} = \vec{I} + \vec{S}$ along the z axis. The states are

chosen recognizing that only the states with the same F value will interfere. The angles η,$\epsilon \in [0, \pi/2]$ determine the relative populations, and $\beta, \gamma \in [0, 2\pi]$ the relative phases of the superposition.
In this case, the value of the control index (Eq. (26)) is 0.83, showing the robustness of control. We find that the minimum value of the total cross section (see Fig.2 (a)) is 11 times smaller than the maximal value (24,669 and 263,065 Å^2 respectively).

Here, the control is less effective than for the case of the scattering of oxygen molecules, but the advantage of the rubidium case is in experimental implementation. That is, ultracold rubidium atoms are widely available in optical dipole traps [42, 43] or, more recently, in optical tweezer setups [44]. Furthermore, initial steps toward the creation of entangled superposition similar to Eq.(30) between two ^{85}Rb atoms have been demonstrated in optical tweezers[44]. However, in these experiments a magnetic field is applied to lift the degeneracy, which would prevent the interference-based coherent control. In that case only the low-magnetic field regime would be appropriate for control. In general, however, the difficulty associated with coherent control from initial entangled states is that it is a two step process, collisional creation of the entangled state followed by the subsequent controlled collision. Despite the experimental challenges associated with this approach we have examined the entangled case since it is formally and conceptually instructive.

C. Non-entangled superpositions

The preparation of entangled superpositions (Eq. 28 and 30) does pose an experimental challenge. However, entanglement is not a necessary condition for control. Below we consider control in the scattering of independently prepared molecules.

For the case of O_2+O_2 collisions, the two colliding molecules are prepared in two different superpositions:

$$|\psi_A\rangle = N\left(\sqrt{\cos\eta}\,|1,-1\rangle + \sqrt{\sin\eta}\,e^{i\frac{\beta}{2}}\,|1,0\rangle\right) e^{ik_A z_A} e^{i\alpha_A} \tag{31}$$

$$|\psi_B\rangle = N\left(\sqrt{\sin\eta}\,e^{i\frac{\beta}{2}}\,|1,0\rangle + \sqrt{\cos\eta}\,|1,1\rangle\right) e^{ik_B z_B} e^{i\alpha_B}, \tag{32}$$

where $N = (\sin\eta + \cos\eta)^{-1/2}$ is a normalization factor. $k_A(k_B)$ and z_A (z_B) are the momentum and the position of the particle A (B), respectively. α_A and α_B are global phases related to the preparation time of the superposition. Here, for simplicity, we consider states of A and B with population and relative phase in both being determined by the same parameter η and β. Different choices of control parameters in A and B are also possible.

The initial superposition is then obtained by symmetrizing the product $|\psi_A\rangle\,|\psi_B\rangle$ to give in the relative motion frame :

$$\begin{aligned}\Psi_{NE}(\vec{r},\xi) = N^2 e^{ikz} e^{i(\alpha_A+\alpha_B)} \\ \Big[\cos\eta\,|1,-1,1,1\rangle + \sin\eta\,e^{i\beta}\,|1,0,1,0\rangle \\ + \sqrt{\cos\eta\,\sin\eta}\,e^{i\frac{\beta}{2}}(|1,-1,1,0\rangle + |1,0,1,1\rangle)\Big].\end{aligned} \tag{33}$$

Note that the phases α_A and α_B still act as global phases and hence do not have any effect on the control.

Preparation at the level of the individual molecules implies that the superposition contains a range of states with different values of M_{int}. Here, there are two states with $M_{int} = 0$, one state with $M_{int} = 1$, and one state with $M_{int} = -1$. Since these supplementary states do not interfere, they are termed satellite states [23]. The main difference with the entangled cases is the elastic contributions from the initial satellite states $|1,-1,1,0\rangle$ and $|1,0,1,1\rangle$. This elastic scattering was absent for the control of the state-to-state cross section to $|1,-1,1,+1\rangle$ and $|1,0,1,0\rangle$ in our previous study [25] but must be included in the control of the total cross section. Fortunately, the elastic cross section is equal 782.7 Å^2, almost two orders of magnitude lower than the other contributions in the total cross section. For example, with $\eta = \pi/4$ fixed (see Fig. 1(d)), coherent control of the total cross section by varying the relative phase is still extensive, with a factor of 41 between the maximal and minimal values. Therefore, even with a non-entangled superposition, it is possible to substantially control the total cross section for O_2 + O_2 scattering.

As an example in the Rb + Rb case, the two colliding atoms are prepared in two different three-state superpositions:

$$\begin{aligned}|\psi_A\rangle = N_3\Big(&\sqrt{\sin\eta\,\sin\epsilon}\,|2,-2\rangle \\ &+\sqrt{\cos\eta\,\sin\epsilon}\,e^{i\frac{\beta}{2}}\,|2,-1\rangle \\ &+\sqrt{\cos\epsilon}\,e^{i\frac{\gamma}{2}}\,|2,0\rangle\Big) e^{ik_A z_A} e^{i\alpha_A},\end{aligned} \tag{34}$$

$$\begin{aligned}|\psi_B\rangle = N_3\Big(&\sqrt{\sin\eta\,\sin\epsilon}\,|2,2\rangle \\ &+\sqrt{\cos\eta\,\sin\epsilon}\,e^{i\frac{\beta}{2}}\,|2,1\rangle \\ &+\sqrt{\cos\epsilon}\,e^{i\frac{\gamma}{2}}\,|2,0\rangle\Big) e^{ik_B z_B} e^{i\alpha_B},\end{aligned} \tag{35}$$

where $N_3 = (\sin\eta\,\sin\epsilon + \cos\eta\,\sin\epsilon + \cos\epsilon)^{-1/2}$.
As in the oxygen case, the initial non-entangled superposition is obtained by symmetrizing the product

$|\psi_A\rangle\,|\psi_B\rangle$:

$$\Psi_{NE}(\vec{r},\xi) = N_3^2\,\mathrm{e}^{ikz}\mathrm{e}^{i(\alpha_A+\alpha_B)}\Big[\cos\eta\,\sin\epsilon\,|2,-2,2,2\rangle + \sin\eta\,\sin\epsilon\,\mathrm{e}^{i\beta}\,|2,-1,2,1\rangle + \cos\epsilon\,\mathrm{e}^{i\gamma}\,|2,0,2,0\rangle + \sqrt{\sin\eta\,\cos\eta}\,\sin\epsilon\,\mathrm{e}^{i\frac{\beta}{2}}(|2,-2,2,1\rangle + |2,-1,2,2\rangle) + \sqrt{\sin\eta\,\sin\epsilon\,\cos\epsilon}\,\mathrm{e}^{i\frac{\gamma}{2}}(|2,-2,2,0\rangle + |2,0,2,2\rangle) + \sqrt{\cos\eta\,\sin\epsilon\,\cos\epsilon}\,\mathrm{e}^{i\frac{\beta+\gamma}{2}}(|2,-1,2,0\rangle + |2,0,2,1\rangle)\Big]. \tag{36}$$

In this case, there are four groups of states: one group of three states with $M_{int}=0$, two groups of two states with $M_{int}=\pm1$ and two groups of one state with $M_{int}=\pm2$. The total cross section is the sum of the ICS correspondingly to each group. The two last terms are uncontrollable and give a large contribution due to the elastic cross section. Moreover, the groups of initial states with $M_{int}=\pm1$ have a different control landscape than the group with $M_{int}=0$, affecting the control.

Coherent control by varying the relative phases is shown in Figure 2 (b). Here, the ratio max/min is significantly reduced,relative to the entangled case, to a factor of two (163,911 and 74,512 Å^2 respectively). With the non-entangled superposition, the quasi-vanishing of the total cross section is lost. This difference between the oxygen and rubidium cases arises from the number of uncontrollable "satellite" terms [23], prevalent in Eq. (36). Nevertheless, if the cross section can be accurately measured, the predicted control is sufficiently large to be experimentally measurable.

VI. CONCLUSION

We derived the coherent multichannel optical theorem for the scattering of initial coherent superpositions, a fundamental contribution to scattering theory, introducing new interference contributions. As an example, it was then used to address three issues. The first was to determine how the coherent multichannel optical theorem reflects contributions from an initial superposition of internal states. As in the standard form of the optical theorem, the forward scattering plays an essential role. However, the extended theorem shows that inelastic scattering between the states involved in the initial superpositions is crucial in the optical theorem and here in applications to the coherent control of the total integral cross section.

The second issue concerned optical theorem insights into the coherent control of the total scattering cross section. The maximal and the minimal values of the total cross sections were found to be directly related to the elastic and inelastic forward scattering amplitudes. If these quantities fulfill the Schwartz equality, the minimal value vanishes and complete control is possible. Furthermore, the Schwartz equality allowed us to define a control index through which the extent of control can be understood. These statements were generalized to include the initial superpositions of N_{sup} internal states of the collision partners.

Finally, the third issue concerned identifying cold atomic and molecular collision systems with a large extent coherent control to motivate experimental demonstrations of coherent control of scattering. Two interesting cases were examined: O_2+O_2 scattering in their rovibrational ground state, and the scattering of rubidium atoms ^{85}Rb. To examine experimental requirements on the initial state preparation, we considered both entangled and non-entangled superpositions, where the latter could be created by preparation of the individual molecules. Although the entangled states display greater control, the non-entangled initial superpositions show sufficient control to be both significant and experimentally observable. Ultracold O_2+O_2 scattering was found to allow better control, while ultracold ^{85}Rb+^{85}Rb collisions could be easier to probe experimentally, given widespread availability of ultracold Rb atoms in either optical dipole traps [42, 43] or optical tweezers [44]. These two cases demonstrate that a large degree of control can be obtained for multi-channel scattering, and motivate the first experimental demonstration of the quantum interference based control of the total cross section in ultracold atomic and molecular collisions.

ACKNOWLEDGEMENTS

This work was supported by the U.S. Air Force Office of Scientific Research (AFOSR) under Contract No. FA9550-19-1-0312. SciNet computational facilities are gratefully acknowledged.

APPENDIX A: CALCULATION OF THE INCOMING FLUX

The incoming current density for the superposition state takes the form:

$$\vec{j}_{in}(\vec{r}) = \left[\int \mathrm{d}\xi \frac{\hbar}{2i\mu}\left(\sum_{i=1}^{N_{sup}} a_i\,|i\rangle\,\mathrm{e}^{ikz}\right)^* \vec{\nabla}\left(\sum_{i'=1}^{N_{sup}} a_{i'}\,|i'\rangle\,\mathrm{e}^{ikz}\right)\right] + \text{c.c.} \tag{37}$$

Using the orthogonality of the channel basis states $\langle i|i'\rangle = \delta_{i,i'}$ and $\sum_{i=1}^{N_{sup}}|a_i|^2 = 1$, one obtains:

$$\vec{j}_{in}(\vec{r}) = \frac{\hbar k}{\mu}\hat{e}_z, \tag{38}$$

where $\hat{e}_z$ is the unit vector along $\vec{z}$.
The integral on the closed surface gives:

$$I_{in} = \lim_{r\to\infty} r^2 \frac{\hbar k}{\mu}\int \hat{e}_z\cdot\hat{e}_r \mathrm{d}\Omega, \tag{39}$$

$$I_{in} = \lim_{r\to\infty} r^2 \frac{\hbar k}{\mu} 2\pi \int_0^\pi \sin\theta \, \cos\theta \mathrm{d}\theta. \tag{40}$$

Since $\int_0^\pi \sin\theta \, \cos\theta \mathrm{d}\theta = 0$, the incoming contribution vanishes:

$$I_{in} = 0. \tag{41}$$

APPENDIX B: CALCULATION OF THE OUTGOING FLUX

The outgoing current density is:

$$\vec{j}_{out}(\vec{r}) = \left[\int \mathrm{d}\xi \frac{\hbar}{2i\mu} \left(\sum_j f_{sup\to j}(\theta,\phi) \frac{\mathrm{e}^{ik_j r}}{r} |j\rangle \right)^* \vec{\nabla} \left(\sum_{j'} f_{sup\to j'}(\theta,\phi) \frac{\mathrm{e}^{ik_{j'} r}}{r} |j'\rangle \right) \right] + \text{c.c.} \tag{42}$$

Using the orthogonality relation, equation (42) becomes:

$$\vec{j}_{out}(\vec{r}) = \frac{\hbar}{\mu} \sum_j \frac{k_j}{r^2} |f_{sup\to j}(\theta,\phi)|^2 \hat{e}_r + O\left(\frac{1}{r^3}\right). \tag{43}$$

Note that the angular components of the gradient operator (included in $O\left(\frac{1}{r^3}\right)$) have been neglected. Indeed, when the limit of r to infinity is taken, those angular components become negligible in comparison to the radial component.

The integrated quantity takes the form:

$$I_{out} = \frac{\hbar}{\mu} \sum_j k_j \int |f_{sup\to j}(\theta,\phi)|^2 \mathrm{d}\Omega. \tag{44}$$

Using the definitions of the differential cross section , $\frac{d\sigma_{sup}}{d\Omega} = \frac{k_j}{k} |f_{sup\to j'}(\theta,\phi)|^2$, and of the total ICS, $\sigma_{sup}^{tot} = \sum_j \int \frac{d\sigma_{sup}}{d\Omega} d\Omega$, I_{out} becomes:

$$I_{out} = \frac{\hbar k}{\mu} \sigma_{sup}^{tot}. \tag{45}$$

APPENDIX C: CALCULATION OF THE INTERFERING FLUX

The interference current density takes the form:

$$\begin{aligned} \vec{j}_{int}(\vec{r}) = \Bigg[\int \mathrm{d}\xi \frac{\hbar}{2i\mu} \left(\sum_{i=1}^{N_{sup}} a_i |i\rangle \, \mathrm{e}^{ikz} \right)^* \\ \vec{\nabla} \left(\sum_j f_{sup\to j}(\theta,\phi) \frac{\mathrm{e}^{ik_j r}}{r} |j\rangle \right) \\ + \frac{\hbar}{2i\mu} \left(\sum_j f_{sup\to j}(\theta,\phi) \frac{\mathrm{e}^{ik_j r}}{r} |j\rangle \right)^* \\ \vec{\nabla} \left(\sum_{i=1}^{N_{sup}} a_i |i\rangle \, \mathrm{e}^{ikz} \right) \Bigg] + \text{c.c.} \end{aligned} \tag{46}$$

After the applications of the gradient and the orthogonality relation, the interference current density becomes:

$$\begin{aligned} \vec{j}_{int}(\vec{r}) = \Bigg[\frac{\hbar}{2\mu} \sum_i^{N_{sup}} a_i^* f_{sup\to i}(\theta,\phi) \mathrm{e}^{ikr(1-\cos\theta)} \\ \left[\frac{k}{r}(1+\cos\theta) + \frac{i}{r^2} \right] \hat{e}_r \Bigg] + \text{c.c.} \end{aligned} \tag{47}$$

As for the outgoing contribution, only the radial component of the gradient is considered. The integral on the closed surface is equal to:

$$\begin{aligned} I_{int} = \Bigg[\frac{\hbar}{2\mu} \sum_i^{N_{sup}} a_i^* \lim_{r\to\infty} \int_0^{2\pi} d\phi \int_0^\pi \mathrm{d}\theta \, \sin\theta f_{sup\to i}(\theta,\phi) \\ \mathrm{e}^{ikr(1-\cos\theta)} \left[rk(1+\cos\theta) + i \right] \Bigg] + \text{c.c.} \end{aligned} \tag{48}$$

Due to the uniform convergence of the limit, the order of the integral on ϕ and the limit on r can be interchanged. We focus in the θ integral first. Then, two limits must be calculated:

$$\lim_{r\to\infty} rk \int_0^\pi \mathrm{d}\theta \, \sin\theta f_{sup\to i}(\theta,\phi) \mathrm{e}^{ikr(1-\cos\theta)} (1+\cos\theta), \tag{49}$$

$$\lim_{r\to\infty} i \int_0^\pi \mathrm{d}\theta \, \sin\theta f_{sup\to i}(\theta,\phi) \mathrm{e}^{ikr(1-\cos\theta)}. \tag{50}$$

We consider the second limit(50) and we make the changes of variables $x = 1-\cos\theta$ and $\kappa = kr$. We also, for notational clarity, suppress the ϕ dependence of $f_{sup\to i}(\theta,\phi)$ until Eq.(59). Eq. (50) then becomes:

$$\begin{aligned} \lim_{r\to\infty} \int_0^\pi \mathrm{d}\theta \, \sin\theta f(\theta) \mathrm{e}^{ikr(1-\cos\theta)} = \\ \lim_{\kappa\to\infty} \int_0^2 \mathrm{d}x f(x) \mathrm{e}^{i\kappa x}. \end{aligned} \tag{51}$$

By the Riemann-Lebesgue lemma, this limit vanishes:

$$\lim_{\kappa\to\infty}\int_0^2 \mathrm{d}x f(x)\mathrm{e}^{i\kappa x}=0. \tag{52}$$

Now, we focus on the limit (49) and make the same change of variables:

$$\lim_{r\to\infty} kr\int_0^\pi \mathrm{d}\theta\,\sin\theta f(\theta)\mathrm{e}^{ikr(1-\cos\theta)}(1+\cos\theta)= \lim_{\kappa\to\infty}\kappa\int_0^2 \mathrm{d}x f(x)\mathrm{e}^{i\kappa x}(2-x). \tag{53}$$

After integration by parts, we obtain:

$$\lim_{\kappa\to\infty}\kappa\int_0^2 \mathrm{d}x f(x)\mathrm{e}^{i\kappa x}(2-x)= \frac{1}{i}\left(\lim_{\kappa\to\infty}[f(x)(2-x)\mathrm{e}^{i\kappa x}]_0^2 - \lim_{\kappa\to\infty}\int_0^2 (f(x)(2-x))'\mathrm{e}^{i\kappa x}\mathrm{d}x\right). \tag{54}$$

Using the Riemann-Lebesgue lemma, the second term evaluates to zero:

$$\lim_{\kappa\to\infty}\kappa\int_0^2 \mathrm{d}x f(x)\mathrm{e}^{i\kappa x}(2-x)= \frac{1}{i}\left(\lim_{\kappa\to\infty}[f(x)(2-x)\mathrm{e}^{i\kappa x}]_0^2\right). \tag{55}$$

The first term gives:

$$\lim_{\kappa\to\infty}\kappa\int_0^2 \mathrm{d}x f(x)\mathrm{e}^{i\kappa x}(2-x)=\frac{-2f(x=0)}{i}, \tag{56}$$

$$\lim_{\kappa\to\infty}\kappa\int_0^2 \mathrm{d}x f(x)\mathrm{e}^{i\kappa x}(2-x)=2if(x=0). \tag{57}$$

$x=0$ corresponds to $\theta=0$. Therefore, one obtains:

$$\lim_{r\to\infty} kr\int_0^\pi \mathrm{d}\theta\,\sin\theta f(\theta)\mathrm{e}^{ikr(1-\cos\theta)}(1+\cos\theta)= 2if(\theta=0). \tag{58}$$

Then, I_{int} becomes, where we restore the ϕ dependence in f and consider the ϕ integral:

$$I_{int}=\frac{i\hbar}{\mu}\sum_i^{N_{sup}} a_i^*\int_0^{2\pi}\mathrm{d}\phi f_{sup\to i}(\theta=0,\phi)+\text{c.c.} \tag{59}$$

The forward scattering amplitudes from the superposition $f_{sup\to i}(\theta=0,\phi)$ is then expanded in state-to-state scattering amplitudes (see Eq. (3)):

$$I_{int}=\frac{i\hbar}{\mu}\sum_{i,i'=1}^{N_{sup}} a_i^* a_{i'}\int_0^{2\pi}\mathrm{d}\phi f_{i'\to i}(\theta=0,\phi)+\text{c.c.} \tag{60}$$

The forward scattering amplitude does not depend on ϕ, so that the integral on ϕ simply gives:

$$I_{int}=\frac{2\pi i\hbar}{\mu}\sum_{i,i'=1}^{N_{sup}} a_i^* a_{i'} f_{i'\to i}(\theta=0)+\text{c.c}, \tag{61}$$

$$I_{int}=\frac{-4\pi\hbar}{\mu}\sum_{i,i'=1}^{N_{sup}} \mathrm{Im}[a_i^* a_{i'} f_{i'\to i}(\theta=0)]. \tag{62}$$

APPENDIX D: DETAILS OF THE NUMERICAL CALCULATIONS

O_2+O_2 scattering

We perform quantum scattering calculations on O_2 + O_2 collisions using a coupled-channel (CC) methodology [45] based on the expansion of the scattering wavefunction in an uncoupled symmetrized space-fixed basis set composed of direct products of molecular rotational and spin basis functions and the orbital angular momentum eigenstates. Most of the computational details are essentially the same as reported in the previous work of one of the authors [45]. The CC basis set was composed of three rotational states ($N=0-4$) and 6 partial waves ($\ell=0-10$) at 10 μK. The hyperfine structure of $^{17}O_2$ was neglected to make the calculations computationally feasible. The CC equations were integrated on the radial grid from $R_{\min}=4.0\,a_0$ to $R_{\max}=150\,a_0$ with a grid step of $0.04\,a_0$. The T-matrix elements are obtained from this CC results and are used to calculate the forward scattering amplitudes:

$$f_{i\to j}(\theta=0)=\frac{1}{2k}\sum_\ell\sum_{\ell'} i^{\ell-\ell'+1}\sqrt{(2\ell+1)(2\ell'+1)}T_{i\ell 0\to j\ell' 0}. \tag{63}$$

Finally, the total cross section is calculated using the coherent multichannel optical theorem (Eq. 12).

Rb+Rb scattering

Quantum scattering calculations of ultracold ^{85}Rb+^{87}Rb collisions were performed following the same methodology as in the previous works [41, 46, 47]. The CC equations were integrated on the radial grid from $R_{\min}=2.0\,a_0$ to $R_{\max}=300\,a_0$ with a grid step of $0.005\,a_0$. The calculation of the forward scattering amplitude and of the total cross section is the same as that for O_2-O_2 scattering.

[1] J. R. Taylor, *Scattering Theory: The Quantum Theory of Nonrelativistic Collisions* (John Wiley & Sons, 1972).
[2] H. Friedrich, *Scattering Theory* (Springer, 2013).
[3] E. Sellmeier, Zur erklärung der abnormen farbenfolge in spectrum einiger substanzen, Ann. Phys. Chem. **143**, 272 (1871).
[4] L. Rayleigh, On the light from the sky, its polarization and colour, Philos. Mag. **47**, 375 (1871).
[5] E. Feenberg, The scattering of slow electrons by neutral atoms, Phys. Rev. **40**, 40 (1932).
[6] N. Bohr, R. Peierls, and G. Placzek, Nuclear reactions in the continuous energy region, Nature **144**, 200 (1939).
[7] K. N. Joshipuraand P. M. Patel, Total electron scattering cross sections for NO, CO, NO_2, N_2O, CO_2 and NH_3. (Ei > 50 eV), J. Phys. B: A. Mol. Opt. Phys. **29**, 3925 (1996).
[8] Y. Jiang, J. Sun, and L. Wan, Total cross sections for electron scattering by polyatomic molecules at 10-1000 eV: C_2H_2, C_2H_4, C_2H_6, C_3H_6, C_3H_8 and C_4H_8, Z. Phys. D **34**, 29 (1995).
[9] T. Scholz, H. R. J. Walters, and P. G. Burke, The total cross section for electron scattering by atomic hydrogen, J. Phys. B: A. Mol. Opt. Phys. **23**, L467 (1990).
[10] Y. E. Kim, Y. J. Kim, and A. L. Zubarev, Optical theorem formulation of low-energy nuclear reactions, Phys. Rev. C **55**, 801 (1997).
[11] R. Lipperheide, Heavy-ion reaction cross sections from elastic scattering data, Nuclear Physics , 190 (1987).
[12] T. Udagawaand T. Tamura, Derivation of breakup-fusion cross sections from the optical theorem, Phys. Rev. C **24**, 1348 (1980).
[13] G. Pancheriand Y. N. Srivastava, Introduction to the physics of the total cross section at LHC, Eur. Phys. J. C. **77**, 150 (2016).
[14] W. C. S. R. V. Kremsand B. Friedrich, *Cold Molecules* (CRC Press, 2009).
[15] M. Karra, K. Sharma, B. Friedrich, S. Kais, and D. Herschbach, Prospects for quantum computing with an array of ultracold polar paramagnetic molecules, J. Chem. Phys. **144**, 094301 (2016).
[16] J. W. Park, Z. Z. Yan, H. Loh, S. A. Will, and M. W. Zwierlein, Second-scale nuclear spin coherence time of ultracold $^{23}Na^{40}K$ molecules, Science **357**, 372 (2017).
[17] P. Yu, L. W. Cheuk, I. Kozyryev, and J. M. Doyle, A scalable quantum computing platform using symmetric-top molecules, New J. Phys. **21**, 093049 (2019).
[18] V. V. Albert, J. P. Covey, and J. Preskill, Robust encoding of a qubit in a molecule, Phys. Rev. X **10**, 031050 (2020).
[19] L. D. Carr, D. DeMille, R. V. Krems, and J. Ye, Cold and ultracold molecules: science, technology and applications, New J. Phys. **11**, 055049 (2009).
[20] B. Heazlewoodand T. P. Softley, Towards chemistry at absolute zero, Nat. Rev. Chem. **5**, 125–140 (2021).
[21] C. Chin, R. Grimm, P. Julienne, and E. Tiesinga, Feshbach resonances in ultracold gases, Rev. Mod. Phys. **82**, 1225 (2010).
[22] R. V. Krems, *Molecules in Electromagnetic Fields* (Wiley-VCH, 2019).
[23] M. Shapiroand P. Brumer, *Quantum Control of Molecular Processes* (Wiley-VCH, 2012).
[24] H. Zhou, W. E. Perreault, N. Mukherjee, and R. N. Zare, Quantum mechanical double slit for molecular scattering, Science **374**, 960 (2021).
[25] A. Devolder, P. Brumer, and T. V. Tscherbul, Complete quantum coherent control of ultracold molecular collisions, Phys. Rev. Lett. **126**, 153403 (2021).
[26] T. Zelevinski, S. Kotochigova, and J. Ye, Precision test of mass-ratio variations with lattice-confined ultracold molecules, Phys. Rev. Lett. **100**, 043201 (2008).
[27] S. Kotochigova, T. Zelevinski, and J. Ye, Prospects for application of ultracold Sr_2 molecules in precision measurements, Phys. Rev. A **79**, 012504 (2009).
[28] L. Zhu, V. Kleiman, X. Li, S. P. Lu, K. Trenteiman, and R. J. Gordon, Coherent laser control of the product distribution obtained in the photoexcitation of HI, Science **270**, 77 (1995).
[29] M. Shapiroand P. Brumer, Coherent control of collisional events: Bimolecular reactive scattering, Phys. Rev. Lett. **77**, 2574 (1996).
[30] A. Abrashkevich, M. Shapiro, and P. Brumer, Coherent control of atom-diatom reactive scattering: isotopic variants of $H+H_2$ in three dimensions, Chem. Phys. **267**, 81 (2001).
[31] J. Gong, M. Shapiro, and P. Brumer, Entanglement-assisted coherent control in nonreactive diatom–diatom scattering, J. Chem. Phys. **118**, 2626 (2003).
[32] V. Zeman, M. Shapiro, and P. Brumer, Coherent control of resonance-mediated reactions: F + HD, Phys. Rev. Lett. **92**, 133204 (2004).
[33] P. Brumer, A. Abrashkevich, and M. Shapiro, Laboratory conditions in the coherent control of reactive scattering, Faraday Discuss. **113**, 291 (1999).
[34] W. E. Perreault, N. Mukherjee, and R. N. Zare, Quantum control of molecular collisions at 1 Kelvin, Science **358**, 356 (2017).
[35] W. E. Perreault, N. Mukherjee, and R. N. Zare, Cold quantum-controlled rotationally inelastic scattering of HD with H_2 and D_2 reveals collisional partner reorientation, Nat. Chem. **10**, 561 (2018).
[36] N. Mukherjee, W. Dong, and R. Zare, Coherent superposition of m-states in a single rovibrational level of H_2 by Stark-induced adiabatic raman passage, J. Chem. Phys. **140**, 074201 (2014).
[37] Y. Liu, M.-G. Hu, M. A. Nichols, D. Yang, D. Xie, H. Guo, and K.-K. Ni, Precision test of statistical dynamics with state-to-state ultracold chemistry, Nature **593**, 379 (2021).
[38] B. Margulis, J. Narevicius, and E. Narevicius, Direct observation of a Feshbach resonance by coincidence detection of ions and electrons in Penning ionization collisions, Nature Communications **11**, 3553 (2020).
[39] E. Frishman, M. Shapiro, and P. Brumer, Coherent enhancement and suppression of reactive scattering and tunneling, J. Chem. Phys. **110**, 9 (1999).
[40] Y. Segev, M. Pitzer, M. Karpov, N. Akerman, J. Narevicius, and E. Narevicius, Collisions between cold molecules in a superconducting magnetic trap, Nature **572**, 189 (2019).
[41] R. Hermsmeier, A. Devolder, P. Brumer, and T. V. Tscherbul, Near-threshold scaling of resonant inelastic collisions at ultralow temperatures, arXiv: https://arxiv.org/abs/2105.11995 (2021).

[42] R. Grimm, M. Weidemüller, and Y. B. Ovchinnikov, Optical dipole traps for neutral atoms, Adv. At. Mol. Opt. Phys. **42**, 95 (2000).

[43] P. Courteille, R. S. Freeland, D. J. Heinzen, F. A. van Abeelen, and B. J. Verhaar, Observation of a Feshbach resonance in cold atom scattering, Phys. Rev. Lett. **81**, 69 (1998).

[44] P. Sompet, S. S. Szigeti, E. Schwartz, A. S. Bradley, and M. F. Andersen, Thermally robust spin correlations between two ^{85}Rb atoms in an optical microtrap, Nature Communications **10**, 1889 (2019).

[45] T. V. Tscherbul, Y. V. Suleimanov, V. Aquilanti, and R. V. Krems, Magnetic field modification of ultracold molecule–molecule collisions, New J. Phys. **11**, 055021 (2009).

[46] Z. Liand R. V. Krems, Electric-field-induced Feshbach resonances in ultracold alkali-metal mixtures, Phys. Rev. A **75**, 032709 (2007).

[47] Z. Li, S. Singh, T. V. Tscherbul, and K. W. Madison, Feshbach resonances in ultracold ^{85}Rb−^{87}Rb and ^{6}Li−^{87}Rb mixtures, Phys. Rev. A **78**, 022710 (2008).